PARAMETERIZATION OF MEAN RESIDENCE TIMES IN IDEALIZED RECTANGULAR DEAD ZONES REPRESENTATIVE OF NATURAL STREAMS

Kevin J. Drost, Sourabh V. Apte[1], Roy Haggerty[2], and Tracie Jackson[3]

ABSTRACT

Three-dimensional Reynolds averaged Navier-Stokes modeling, validated against experimental data, is used to parameterize the flow features and time scales in idealized rectangular cavities for a wide range of width-to-length ratios, $0.4 \leq W/L \leq 1.1$, and Reynolds number based on the depth, $5000 \leq Re_D \leq 20300$, representative of isolated dead zones in small natural streams. The flow features for this parameter range are similar to open cavity flows and consist of a mixing layer spanning the entire length of the dead zone together with a single main recirculation region. The Langmuir time scale (ratio of dead zone volume to discharge) based on the assumption of a well-mixed dead zone is found to be a function of the mean rotation time scale (inverse of average rotation rate) within the dead zone, the momentum thickness of the upstream boundary layer, and the dead zone width. The entrainment coefficient, used to relate the exchange velocity to the average free- stream velocity, is shown to be directly related to the upstream boundary layer momentum thickness non-dimensionalized by the width of the dead zone. Using passive tracer to quantify the mean residence time showed that the dead zone can be characterized by two perfectly mixed regions including a core or secondary region around the center of the eddy and a surrounding primary region that interacts directly with the free-stream through the mixing layer. A two-region model is

[1]School of Mechanical, Industrial, and Manufacturing Engineering, Oregon State University, 204 Rogers Hall, Corvallis, OR 97331.

[2]College of Earth, Ocean, and Atmospheric Sciences, Oregon State University, 104 CEOAS Admin Bldg., Corvallis, OR 97331-5503

[3]Water Resources Engineering Program, College of Earth, Ocean, and Atmospheric Sciences, Oregon State University, Corvallis, OR 97331-5503

developed to obtain time scales associated with the primary and secondary regions within the dead zone using an optimization procedure based on the computational data. The time scale associated with the primary region is representative of the Langmuir time scale and is found to be a strong function of the aspect ratio W/L and the Reynolds number. The secondary region time scale represents the long-time asymptotic behavior of the tracer concentration and is found to be a strong function of the dead zone geometric parameters only.

Keywords: Dead Zones/Cavities, Mean Residence Time, Surface Transient Storage, RANS

INTRODUCTION

As complex ecological and fluid systems, streams may contain dead zones which are parts of the surface channel that have zero mean downstream flow and that exchange water with the main channel. These dead zones can be formed by natural erosion and deposition processes as well as anthropogenic structures. Regardless of origin, dead zones, through turbulent mixing processes, provide refugia for aquatic life and provide transient storage for dissolved substances such as nutrients or pollutants introduced by humans. In the case of both nutrients or pollutants, knowledge of dead zone residence time is critical for understanding reactions and how long the solutes stay in the system.

While irregular dead zones found in natural streams can generally be identified by visual inspection, they contain a consistent set of flow and geometric characteristics as shown in Figure 1(a). Figure 1(b) shows a typical dead zone in a small stream caused by a root protruding into the channel. Physically, a dead zone is formed as a cutout into the bank. Separating the dead zone from the main channel flow is a mixing layer where mass and momentum are exchanged, as shown in figure 1(a). The slower moving fluid in the dead zone is caused by the flow separating at the upstream corner of the dead zone. The separation causes recirculation inside the dead zone. Figure 1(c) shows a schematic of the idealized dead zone geometry with streamwise length, L, and transverse width, W. The depth, D, into the paper is assumed uniform for channel and the dead zone; however, in natural dead zones some variations in depths may occur. The recirculation generally takes the form of one large eddy for typical dead zones in streams, but additional eddies can be present depending on the dead zone geometry, width-to-length ratio (W/L), and stream flow rate or Reynolds number ($Re_D = UD/\nu$), where U is the average free-stream velocity and ν is the kinematic viscosity.

There are two broad types of dead zones that have been studied, those formed by obstructions protruding into the main flow and those formed by cutouts into the bank. The cutout type involves a cavity in the bank of the stream. The flow separates at the beginning of the cavity and recirculates within the dead zone. The obstruction type is formed by a protrusion into the main channel that causes the flow to accelerate. This acceleration leads to larger flow separation and higher velocity gradients near the upstream corner of the dead zone. Obstruction type dead zones are characteristic of erosion control structures or a down tree extending into the channel. Cavity type dead zones are common in natural streams and field work has found that they generally have aspect ratios (W/L) less than one (Jackson et al. 2012).

The transport phenomena involved in dead zones (Valentine and Wood 1979; Gualtieri et al. 2010) are similar to flow features observed in cavity flows relevant to many engineering applications. Of importance are contaminant mass exchange processes in river embayments and main channels (Chang et al. 2006; Engelhardt et al. 2004), shear layer instabilities and relevant heat and momentum transfer processes over aircraft wings (Lin and Rockwell 2001; Lawson and Barakos 2011), and cavitation due to impingement of the shear layer on downstream end of the cavity in naval applications (Liu and Katz 2008).

In studying the mixing properties of turbulent flows, residence times can be important descriptors of the system (Nauman 2008; Levenspiel 1967). The flow characteristics of the mixing layer, the recirculation within the dead zone and the geometry of the dead zone can significantly affect the overall behavior of the system and mean residence times. Currently, researchers use labor-intensive tracer tests to determine the residence time of dead zones experimentally (Gooseff et al. 2005). The response of an entire stream system to a release of a dissolved substance would require the analysis of many individual dead zones. Therefore, it is important to develop simplified yet accurate models of the transport processes that occur within a dead zone. The goal of these simplified models would be to facilitate quick and accurate estimation of the appropriate residence times associated with a given dead zone.

The objective of this work is to characterize the time scales present in an idealized dead zone. In general, each time scale is a function of the relevant nondimensional groups, Re_D, W/L, W/D, and Fr. This work explores the nondimensional relationship using parametric numerical studies. Many experiments (Valentine and Wood 1979; Uijttewaal et al. 2001; Weitbrecht et al. 2008) have found that dead zone time scales are approximately two orders of magntitude larger than the time scale of the main stream. A physical explanation for this difference in scales is proposed using simple scaling arguements combined with the parametric results. Such a large parametric study requires the use of an efficient numerical method, Reynolds Averaged Navier Stokes (RANS), as opposed to detailed Large Eddy Simulations (LES). A simplified model is also introduced as an extension of the Continuously Stirred Tank Reactor (CSTR) model. The model parameters lend insight into the transport phenomenon and can be correlated to the important nondimensional groups. Developing this model could help predict dead zone time scales without time consuming field measurements.

This work focuses on dead zones with an idealized rectangular geometry (Figure 1(c)). Range of parameter variation investigated in this work corresponds to the dead zones occurring in natural streams: length ($0.45 \leq L \leq 1.25$ $[m]$), width ($0.5 \leq W \leq 1.25$ $[m]$), depth ($0.023 \leq D \leq 0.092$ $[m]$), and stream mean velocity ($0.11 \leq U \leq 0.248$ $[m/s]$). This varies the Reynolds number based on the depth, $Re_D = DU/\nu$, over the range 5000-20300 and aspect ratio W/L over the range 0.4-1.1 typically observed in natural streams. The depths used correspond to shallow stream levels. For these parameter ranges, the flow features observed consist of a large primary recirculation zone within the cavity. In addition, the mixing layer spans the entire length of the cavity. The developed models are thus only applicable to dead zones with such flow characteristics.

Review of Relevant Studies

As shown in figure 1(a), the flow structure in a dead zone typically involves a mixing layer at one end and a recirculating region within the cavity bounded by walls on three sides and can depend on the flow Reynolds number, the cavity shape, and the aspect ratio (W/L). Lawson and Barakos (2011) found that for low speeds and small aspect ratios (large L), a distinct recirculation region is not observed. The mixing layer does not extend all the way to the downstream corner of the cavity and the flowfield is classified as closed cavity flow. As Re_D is increased and/or W/L is increased, an open cavity flow is obtained. The present work focuses on such open cavity flows.

Weitbrecht et al. (2008) studied the flow patterns inside groyne fields by varying $0.35 \leq W/L \leq 3.4$ for Reynolds number (Re_D) on the order of 7500. They showed that for $W/L < 0.7$, there exist two gyres side-by-side within a cavity: a main primary gyre that is driven by momentum exchange with the main stream and interacts with the mixing layer, and a secondary gyre rotating in the opposite direction and driven by momentum exchange with the primary gyre. The secondary gyre is in contact with the upstream edge of the cavity and has no momentum exchange with the free-stream. For $0.7 \leq W/L \leq 1.5$, the flow structure is replaced by a large single gyre exchanging momentum with the free-stream. For $W/L > 1.5$, the single gyre system becomes unstable, and is replaced by multiple gyres on top of one another. Given these flow regimes, the momentum exchange between the free-stream and the cavity will depend on the aspect ratio.

Open cavity flow structures of dead zones can also be represented by lid-driven cavity flows which have been studied extensively (Koseff and Street 1984; Shankar and Deshpande 2000). Although these types of flows exhibit similar circulation patterns within the cavity, they lack momentum transport across the top boundary as is present in lateral dead zones in streams. The interactions between the mixing layer, the recirculation regions within the cavity, and the free-stream are critical in understanding mass and momentum transfer mechanisms in dead zones.

Several studies have been carried out in quantifying the mass transport in dead zones. Residence times (Nauman 2008; Levenspiel 1967) have been used as important descriptors in quantifying the mixing and transport properties of these turbulent flows. A number of definitions have been used to characterize the mean residence times in dead zones. The hydraulic residence time or Langmuir time scale (τ_L), also called the flushing time or the volumetric time scale, is obtained from the ratio of the volume of the dead zone to the volumetric discharge out of the dead zone (Langmuir 1908; Kozerski et al. 2006; Weitbrecht et al. 2008). The Langmuir time scale, like other dead zone time scales, is inversly proportional to the exchange rate; a small time scale indicates rapid exchange (rapidly decreasing concentration) and vice versa. For a rectangular dead zone with uniform depth equal to the main channel depth, D, the Langmuir time scale is given by

$$\tau_L = \frac{V}{Q} = \frac{WLD}{LDE} = \frac{W}{E}, \tag{1}$$

where V is the volume of the dead zone, Q is the volumetric flow exchanged between the dead zone and the main stream, and E is the average exchange velocity. However, exchange velocity is not known a priori. In order to estimate the exchange velocity, Valentine and Wood (1977) suggest that the entrainment velocity is some fraction of the average main stream velocity, that is $E = k_e U$, where the factor k_e is termed as the entrainment coefficient. This assumption is based on the intermittency of turbulent mixing layer that can be related to the free-stream velocity through some factor. A majority of the research in this field has concentrated on accurately measuring and quantifying the exchange coefficient (Valentine and Wood 1977; Uijttewaal et al. 2001; Kurzke et al. 2002; Kozerski et al. 2006; Chang et al. 2006; Hinterberger et al. 2007; Weitbrecht et al. 2008; McCoy et al. 2008; Constantinescu et al. 2009). However, measurement of exchange velocity and the entrainment coefficient in natural streams is not straightforward.

The entrainment coefficient and the mean residence times can be obtained by use of a conservative tracer experiments that fills the entire dead zone (Gooseff et al. 2005; Briggs et al. 2009). Valentine and Wood (1979) conducted laboratory experiments on simplified dead zones and found that the exchange process can be modeled as a first order system by assuming the dead zone to be perfectly mixed region or CSTR. With the perfectly mixed dead zone assumption, a mass balance can be written for the mass of the passive scalar in the dead zone, as shown in equation 2, where M is the mass of scalar in the dead zone, C is the scalar concentration in the dead zone, and C_{mc} is the constant scalar concentration in the main channel. Using the definition of concentration as mass per unit volume, and assuming the concentration in the main channel is zero, the mass balance turns into a first order differential equation (equation 3). Using the initial concentration difference between the dead zone and the main stream, $(C - C_{mc})_0 = (\Delta C)_0 = C_0$, the differential equation can be solved for the concentration as a function of time (equation 4).

$$\frac{dM}{dt} = -Q\,(C - C_{mc}) = -Q\Delta C \tag{2}$$

$$\frac{dC}{dt} = -\frac{Q}{V}\Delta C = -\frac{E}{W}\Delta C \tag{3}$$

$$\frac{C}{C_0} = \exp\left(-\frac{t}{\tau_L}\right) \text{ where } \tau_L = \frac{W}{E}, \text{ and } E = k_e U \tag{4}$$

The first order model is completely defined by the Langmuir time scale, τ_L. Knowing the time series of concentration, an exponential fit can be applied to a normalized concentration curve to determine the Langmuir time scale. This method gives a single, unique time scale that is a best fit for the entire time series. Valentine & Wood (Valentine and Wood 1977) found that the exchange coefficient was approximately constant for a variety of dead zone geometries. This first order dead zone model was then combined with the axial dispersion model used by Thackston and Schnelle (1970) to model the response of the combination of stream and dead zone.

Recently, Uijttewaal et al. (2001) conducted laboratory flume studies on series of dead zones or groyne fields. The exchange coefficient was generally insensitive to changes in geometry and the flow. Dye concentration studies showed that the system can be approximated as a first order system for early time. At late times, some geometries exhibited a second-order time scale. Particle tracking results show a primary eddy located near the center of the dead zone with a secondary eddy in the upstream corner of the dead zone. The existence of the secondary eddy is hypothesized to contribute an additional time scale to the exchange process.

Weitbrecht et al. (2008) also conducted experiments on a series of dead zones in a laboratory flume. These experiments focused on parametric studies for many different geometric features. Weitbrecht et al. (2008) confirmed that the aspect ratio of the dead zone determines how many eddies will be present. A modified hydraulic diameter, $WL/(W + L)$, was proposed as the effective length scale to combine the geometric terms, and showed that the entrainment coefficient increases with an increasing Reynolds number based on the hydraulic diameter. Their study did not consider the effect of the depth on the entrainment coefficients.

McCoy et al. (2008) further looked at series of dead zones using LES and RANS studies for the same geometry as Uijttewaal et al. (2001). McCoy's results show a clear dependence of the entrainment velocity on depth. Fluid from the main stream tends to be entrained near the bottom surface of the dead zone and at the upstream side. Their work suggests that depth averaging does not appropriately capture the details of the entrainment velocities.

Based on above studies, for flow past rectangular cavities the entrainment coefficient varies over a wide range $0.01 - 0.04$, and considerable uncertainty has been observed in these measurements. These results also indicate that the exchange velocity is two orders of magnitude smaller than the average free-stream velocity. This suggests that different scaling, other than the standard approach of $E = k_e U$, should be possible and needed to relate the exchange velocity to other physical parameters present in the problem. Therefore, a systematic parametric study varying the length, depth, width, and bulk velocity for simple rectangular dead zones can be performed to better quantify their effect on the residence time and is the focus of the present work.

Owing to the complexity of the flow field and mixing process within the dead zone, the simplified first order model has its limitations, as the concentration within the dead zone is not uniform. Engelhardt et al. (2004) conducted large scale experiments on irregularly shaped dead zones in the River Elbe. These experiments showed that the exchange process relies on coherent eddies shed from the upstream corner of the dead zone. Hinterberger et al. (2007) compared depth-averaged LES with full 3D LES and found that the depth averaged simulations predicted significantly higher exchange rates than either 3D LES or experiment. The errors introduced by depth averaging requires that numerical simulations must be three dimensional to accurately predict exchange rates and thus time scales. Kimura and Hosoda (1997a) compared laboratory experiments to numerical results using the depth-averaged equations. The depth averaged equations captured the same average velocity trends as the experiments.

Engelhardt et al. (2004) also found that the exchange process for the irregular dead zones had many time scales and thus could not be represented as a first order system. Additional experiments on the River Elbe by Kozerski et al. (2006) showed that the exchange process is complicated by a dead zone having regions of distinctly different flow characteristics. Under such circumstances, Kozerski et al. (2006) showed that the dead zone can be modeled as a combination of these sub regions. Each sub region is modeled as a first order system.

Bellucci et al. (2001) conducted an analytical investigation of the advection-diffusion equation for semi-enclosed basins assuming a constant eddy diffusivity. The residence times of these basins could be characterized by multiple time scales. Results of the eigenvalue analysis showed that the volume averaged concentration of a passive scalar will always become exponential at late times. Bellucci et al. (2001) showed that the eigenvalue analysis results are applicable to flows with recirculation like dead zones. The characteristic time (T_0) associated with asymptotic exponential decay of the concentration curve has also been used to characterize the residence time (Nauman 2008; Bellucci et al. 2001). A mean residence time

(T_{avg}) can be obtained by the first moment or area under the concentration plot normalized by the initial concentration and is given as, $T_{avg} = \int_0^\infty \frac{C(t)}{C_0} dt$.

The time scales mentioned above (τ_L, T_{avg} and T_0) are generally different for dead zones in natural streams. Recently, Jackson et al. (2012) conducted field experiments on dead zones in natural streams to find considerable variability in obtaining these time scales. This work showed that the dead zone is not perfectly mixed, but has regions marked by primary, secondary, and tertiary eddies, that tend to retain different concentrations of the passive tracer. For a perfectly mixed dead zone $\tau_L = T_{avg} = T_0$. For realistic dead zones, τ_L is the minimum time scale and T_0 is the maximum.

The paper is arranged as follows. The computational approach and its validation with available experimental data on multiple groynes is briefly discussed below. The validated approach is then applied to perform parametric studies on a single dead zone by varying the flow velocity, dead zone width, length, and depth. The main goals of these parameteric studies are (i) to quantify the Languir time scale and the entrainment coefficient by relating them to simple geometric and flow parameters, and (ii) to develop a simple model that can be used to predict the residence time within the dead zone. A two-region model is developed that extends the applicability of standard the first-order model. The parameters for the model are also related to the geometric parameters and flow Reynolds number.

MATHEMATICAL FORMULATION AND COMPUTATIONAL APPROACH

The mathematical formulation is based on Reynolds Averaged Navier Stokes Equations with the standard k-ω model in three dimensions. The k-ω and k-ϵ two equation models are widely used and have been tuned and validated for many different applications including separated flows similar to a dead zone. The k-ω model was selected for its computational efficiency, validation history, and similarity to past work (McCoy et al. 2008). This model introduces two additional transport equations shown in equations 7 and 8, which add computational expense. The time-averaged equations for an incompressible flow are,

$$\frac{\partial \bar{u}_i}{\partial x_i} = 0 \tag{5}$$

$$\frac{\partial \bar{u}_j \bar{u}_i}{\partial x_j} = -\frac{1}{\rho}\frac{\partial P}{\partial x_i} + (\nu + \nu_T)\frac{\partial^2 \bar{u}_i}{\partial x_j \partial x_j}, \tag{6}$$

where ν_T is the eddy viscosity, ν is the kinematic viscosity, P is pressure, and ρ is density. The overbar represents time-averaged quantity. In addition, the turbulence closure for eddy viscosity ($\nu_T = k/\omega$) is obtained by solving the k-ω equations,

$$\overline{u}_j \frac{\partial k}{\partial x_j} = \tau_{ij}\frac{\partial \overline{u}_i}{\partial x_j} - \beta^* k\omega + \frac{\partial}{\partial x_j}\left[(\nu + \sigma^* \nu_T)\frac{\partial k}{\partial x_j}\right] \tag{7}$$

$$\overline{u}_j \frac{\partial \omega}{\partial x_j} = \alpha \frac{\omega}{k}\tau_{ij}\frac{\partial \overline{u}_i}{\partial x_j} - \beta\omega^2 + \frac{\partial}{\partial x_j}\left[(\nu + \sigma^* \nu_T)\frac{\partial \omega}{\partial x_j}\right], \tag{8}$$

where standard model constants are used: $\alpha = 13/25$, $\beta = 9/125$, $\beta^* = 0.09$, $\sigma^* = 0.5$. Once the mean velocity profile is obtained, a transient scalar ($\bar{C}$) advection-diffusion problem is solved by first initializing the dead zone with $\bar{C} = 1$,

$$\frac{\partial \overline{C}}{\partial t} + \overline{u}_j \frac{\partial \overline{C}}{\partial x_j} = \left(\frac{1}{Sc}\nu + \frac{1}{Sc_T}\nu_T\right)\frac{\partial^2 \overline{C}}{\partial x_j \partial x_j}; \qquad Sc_T = \frac{\nu_T}{D_T} \tag{9}$$

where Sc_T is the turbulent Schmidt number (on the order of unity).

The RANS equations are solved for each geometry using the commercial finite volume solver Star-ccm+ (User Guide 2009). The turbulence is modeled using the standard k-ω closure with wall functions. The free surface is modeled as a rigid slip boundary. This approximation is reasonable when the Froude number is small (Fr $<<$ 1) meaning free surface effects are small (Nakayama and Yokojima 2003). The Froude number in the present work ranges between $0.16 <$ Fr < 0.32 and is listed in Table 1. Recent work by (Kimura and Hosoda 1997b) at $Re_D \sim 4500$ and over a range of Froude numbers, showed that the unsteady flow oscillations can become important in mass exchange for $Fr >> 0.33$. However, since the present work deals with higher Reynolds numbers and lower range of Froude numbers, free surface effects are not significant. Similar treatment of the free surface has been used by Hinterberger et al. (2007) and McCoy et al. (2008). All no-slip walls are assumed to be smooth. The bank opposite the dead zone is modeled as a slip wall as its effect is not relevant to this work.

The first step in the solution procedure is to solve for the time averaged steady flow field. Here we use steady RANS approach to obtain the flowfield. In order to confirm that the steady RANS approach predicts the same results, as URANS, a full three-dimensional unsteady RANS study for the baseline case in Table 1 was also conducted. The differences between the steady and unsteady RANS were less than 0.22%. Thus, steady RANS calculations were employed to first obtain the flowfields as it is computationally less intensive. In order to run the passive scalar study, however, a transient simulation is performed by advecting the scalar with the mean steady velocity field and eddy diffusivities. To do this, the time averaged flow field is mapped to the transient simulation and frozen in time. The turbulent Schmidt number is set equal to a value of 0.9 which is the same as Baik et al. (2003), Santiago et al. (2007), and Gualtieri et al. (2010). The passive scalar is initialized with a concentration of one inside the dead zone, up to a line joining the upstream and downstream corners of the dead zone, and zero in the main channel. The average dead zone concentration is calculated as the volume average of all the cells within the dead zone. The initial condition automatically normalizes the concentration to be at one at time zero. The transient simulation is allowed to run until the dead zone concentration is small (~ 0.005), which was found to be on the order of 4000 seconds.

Validation Study

Before using the above approach to perform parametric studies on a single dead zone, detailed validation of the mean flow quantities together with grid refinement study is performed for a series of dead zones for which experimental data are available. Flow in series of dead zones have been studied extensively, both experimentally by Weitbrecht and Jirka (2001), Weitbrecht et al. (2008), and Uijttewaal et al. (2001) and numerically by McCoy et al. (2008), Constantinescu et al. (2009), and Hinterberger et al. (2007). These studies involved series of groynes formed by obstructions protruding into the main flow as well as those formed by cutouts into the bank. The flow separates at the beginning of the cavity and recirculates within the dead zone. The obstruction type is formed by a protrusion into the main channel that causes the flow to accelerate. This acceleration leads to larger flow separation and higher velocity gradients near the upstream corner of the dead zone. Computations involved varying the groyne length to change the aspect ratio, $0.2 \leq W/L \leq 3.4$, as well as varying the freestream velocity to change the Reynolds number ($8000 < Re_D < 39000$). Uijttewaal et al. (2001) conducted experiments on cavity-type dead zones in series which involved different depths in the main stream compared with the dead zone. On the other hand, majority of the data by Weitbrecht et al. (2008) is on protruding-type dead zones with uniform depths in the main stream and the dead zone.

For these cases, systematic grid refinement study was conducted by generating structured grids. Each grid is the most refined in the shear layer between the dead zones and the main channel. The grid coarsens in the spanwise direction away from the dead zone. Near the walls of the dead zone as well as near the stream bed, the grid is refined to obtain a well resolved wall layer. For all cases, the minimum and maximum grid resolution along the depth of the channel is 10 and 78 in wall units. Similar resolutions are within the dead zone as well as inside the mixing layer. First, a periodic, turbulent channel flow is simulated and the mean velocity profile is used as an inlet condition to obtain a fully developed turbulent flow. A no-slip condition is used at the walls and a convective outflow boundary condition is used at the outlet. A slip condition is used at the centerline of the stream.

For all cases, the mean flow, mixing layer characteristics and the dead zone recirculation was compared with the experimental data as well as RANS results by Constantinescu and co-workers (McCoy et al. 2008; Constantinescu et al. 2009) to obtain reasonable agreement (Drost 2012). The mean flow, mixing layer characteristics, and dead zone recirculation compared well with published RANS results. Figure 2 shows the mean streamline patterns predicted for three-different W/L ratios, namely 0.4, 0.77 and 2. For large lengths ($W/L = 0.4$, say), the dead zone has one main eddy that is centered slightly downstream of the dead zone center. There is a secondary eddy in the upstream corner of the dead zone. The secondary eddy has significantly less momentum than the primary eddy. As the dead zone length is decreased, the secondary eddy gets smaller and eventually vanishes around $W/L = 0.77$. As the length is decreased further, the main eddy separates into two eddies stacked in the spanwise direction. Such a flow pattern has been reported experimentally by Weitbrecht et al. (2008) and provides an important qualitative validation of the present predictions. Specifically, predicting the mean flow patterns accurately is critical as that can alter the residence times and scalar dispersion time scales significantly. As will be shown later, majority of the dead zones that occur naturally in the stream fall in the range of W/L that provides a single primary recirculation gyre (similar to the $W/L = 0.4$ case). However, being able to predict the different flow patterns validates the RANS model.

For more quantitative validation, we compare variations of mean velocity and turbulent kinetic energy in the main stream and the dead zone with available experimental data. Figure 3a shows a velocity profile plot in the spanwise direction. This particular case was chosen mainly because it was also studied numerically by McCoy et al. (2008) and thus it allows direct comparison of the present predictions to theirs. In general, the RANS results from the present work matches well to the RANS simulations by McCoy et al. (2008). With refined grids used in the present work, the mean velocity is closer to the experimental data in the main channel. Both RANS profiles differ slightly from the experimental results inside the dead zone. Figure 3b shows a turbulent kinetic energy profile in the spanwise direction. The turbulent kinetic energy (TKE) also shows the same behavior as the experiments, however, the distribution is slightly narrower and the peak in the mixing layer slightly larger in the present predictions compared to the experimental data. The TKE peak is lower and closer to the experimental data in the present simulations compared to that of McCoy et al. (2008). The TKE is a difficult quantity for a RANS model to capture perfectly compared to the experimental data, however, its overall prediction is fairly consistent with experimental measurements. This numerical error is a limitation of the k-ω turbulence model, wherein, all turbulence scales are modeled based on two transport equations. Large eddy simulations (LES) (Constantinescu et al. 2009) are capable of predicting the flowfields much more accurately, however, are computationally intensive. Given a large number of parametric variations conducted in the present work, use of a LES approach is difficult and RANS presents an acceptable tradeoff for the computational efficiency needed.

Finally, to thoroughly validate all aspects of the flow and scalar dispersion, the Langmuir time scale was computed by tracking dispersion of a passive scalar initially uniformly placed within the dead zone. For accurate prediction of the Langmuir time scale, it is critical that the mean flowfield, the turbulent kinetic energy, the exchange mechanisms between the dead zone and the free stream, and the scalar transport are captured correctly. Thus, this quantity helps validate all processes improtant for further analysis to be used in the present work. As W/L is varied over a wide range, the recirculation flow patterns within the dead zone changes significantly and thus can alter the Langmuir time scale. As shown in figure 4, the Langmuir time scales are very well predicted by the RANS results compared to the experimental data (Weitbrecht et al. 2008; Uijttewaal et al. 2001). Here the convective time scale, $T_{conv} = L/U$. Weitbrecht et al. (2008) conducted both particle tracking velocimetry, PTV, and dye concentration, PCA, studies. This validation study establishes sufficient confidence on the predictive capability of the RANS approach for the residence time computations conducted on single dead zones in this study.

PARAMETRIC STUDY RESULTS

This work investigates the time scales that are important to the passive scalar transport within a dead zone. Parametric studies are run by varying the bulk velocity, U and dead zone length, L, width, W, and depth, D. Table 1 shows the parameters used for all of the simulations. The base case is listed first and all additional cases modify a single parameter from the base case. Cases 2-7 vary the length (labeled as L cases), 8-11 vary the velocity (the U cases), 12-14 vary the width (the W cases), and finally 15-17 vary the depth (the D cases). Figure 1(c) shows a planview of the geometries used. The depth is constant throughout the main channel and dead zone. The grid resolution used for these cases was selected to be finer than the validation cases. The minimum grid resolutions in wall units were 1.06 in all directions, whereas the maximum resolution was $\Delta Y^+_{\max} = 59.6$ in the vertical direction and $\Delta X^+_{\max} = \Delta Z^+_{\max} = 119.2$, along the streamwise and spanwise directions, respectively.

Before running simulations with dead zone geometries, a fully developed turbulent inlet condition was generated. Lien et al. (2004) conducted experiments in turbulent channels that could be used to estimate the entrance length. However, adding such a long region to each simulation would greatly increase the computational cost of each simulation. For this work, the inlet condition is generated by simulating a simple periodic channel with the same cross section as the eventual inlet surface. The periodic channel is allowed to evolve until it reaches a stationary state. The inlet condition involving the velocity field and k and ω values are taken from an arbitrary cross section of the periodic channel.

The results from the 17 studies shown in table 1 are used to obtain trends for changes in dead zone geometry and flow conditions. In order to analyze and interpret the results for the various mean residence times, the following time scales are used. The convective time scale, T_{conv} in equation 10, is the time it takes fluid in the main stream to travel the length of the dead zone.

$$T_{conv} = \frac{L}{U}. \tag{10}$$

Typically, the characteristic velocity associated with the mixing layer ($U_m = 0.5U$) is used to define the convective time scale; however, the average free-stream velocity is used here for simplicity. A time scale based on the average rotation rate (Ω) within the dead zone can also be defined,

$$T_{rot} = \frac{1}{\Omega} = \frac{2}{\overline{\omega}_v}. \tag{11}$$

Note that the average rotation rate within the dead zone can be easily obtained from the average vorticity ($\overline{\omega}_v$) which can be obtained by computing the circulation (Γ) within the dead zone.

$$\Gamma = \int \mathbf{u} \cdot \mathbf{d}l = \int_A \omega_v dA = A\overline{\omega}_v, \tag{12}$$

where A is the area of the dead zone, $\overline{\omega_v}$ is the average vorticity within the dead zone, and the mean circulation is computed along a closed path ($\mathbf{d}l$) encompassing the dead zone at the free surface. It is possible to consider an average of circulation evaluated at all planes in the plan view. However, it was done at the free surface mainly because majority of the data collected in field measurements is only at the free surface. In order to verify that the trends are unaltered, we have also estimated Γ based on average of circulation over all planes, and the general trends presented in the paper are not affected significantly.

Entrainment Coefficient Scaling

One of the main goals of parametric studies is to obtain detailed data on the Langmuir time scale, τ_L, and develop a simple relationship for the entrainment coefficient, k_e. As mentioned earlier, the Langmuir time scale depends on the exchange velocity between the main stream and the dead zone and is difficult to measure in the field. Instead, Valentine and Wood (1977) suggest that the entrainment velocity is some fraction of the average main stream velocity, and given by the entrainment coefficient. For a majority of streams and river dead zones, the observed entrainment coefficients are within the range of $0.01 - 0.04$ (Jackson et al. 2012; Jackson et al. 2013). However, a definitive relation between k_e and some measurable geometric and flow parameters of the dead zone is needed.

First, the Langmuir time scale in the first order continuous stirred reactor (CSTR) model, is obtained by using the dead zone geometry and the mean exchange velocity E obtained directly from the steady flowfield predicted by the RANS results, $\tau_L = W/E$. Since the exchange velocity is typically defined through the exchange coefficeint and the mean free-stream velocity, $E = k_e U$, the Langmuir time scale versus W/U is first plotted to obtain nearly a linear relationship as shown in figure 5, the inverse slope of which gives the entrainment coefficient, $k_e \sim 0.01$. This is within the experimental range observed (0.01-0.03) for data on real dead zones in natural streams (Jackson et al. 2012).

The relationship between the Langmuir time scale, the mean free-stream velocity, and the width of the dead zone can also be interpreted using some measure of net circulation within the dead zone. The circulation within the dead zone (equation 12) can be estimated by integrating the velocity along a closed loop encompassing the edges of the dead zone at the free surface and the center of the mixing layer (line joining the upstream and downsteam corners of the dead zone). Using the characteristic mixing layer velocity ($U_m = 0.5U$) as an approximate model to the actual mean streamwise velocity at the center of the mixing layer, the net circulation is simply obtained as,

$$\Gamma \sim U_m L = 0.5UL. \tag{13}$$

Using equation 12, the average vorticity in the dead zone is given as,

$$\overline{\omega}_v = \frac{\Gamma}{A} \sim \frac{0.5UL}{WL} = 0.5\frac{U}{W}. \tag{14}$$

Thus, $W/U \sim 1/(2\overline{\omega}_v)$. This was confirmed by actually computing the average vorticity within the dead zone based on the mean flow field at the free surface. It was found that W/U correlated linearly with $1/\overline{\omega}_v$ for most cases, except for some cases where the length or depth were varied. That is attributed to the fact that, the characteristic mixing layer velocity (U_m) is just an approximate model and may not be the exact velocity along the line joining the upstream and downstream ends of the dead zone. This result suggests that the Langmuir time scale must be related to the rotation time scale, $T_{rot} = 2/\overline{\omega}_v$, and is confirmed as shown in figure 6(a). This figure shows that the Langmuir time scale varies linearly with the rotation time scale and that the fit for all cases is much better than that against W/U shown in figure 5. This physically means that the Langmuir time scale is governed mostly by the average recirculation in the dead zone. Faster circulating fluid will reduce the residence time. The average rotation rate is dependent on the free-stream velocity as well as the geometry of the dead zone, implictly including all main parameters associated with the problem, namely the geometric features L, W, and D, and the average free-stream velocity, U. It should be noted that the inverse slope of the plot of τ_L versus $1/\overline{\omega}_v$ is also related to the entrainment coefficient and shows a value on the order of 0.015.

This relation incorporates the dead zone flow characteristics through the average rotation rate; however, it does not explicitly include the mixing layer parameters. The driving force for the rotation inside the dead zone is the turbulent boundary layer upstream of the dead zone or the bed shear stress. The boundary layer is well characterized by the momentum thickness (θ) as defined in equation 15 where u is the average streamwise velocity as a function of the distance away from the wall and u_0 is the average streamwise velocity far from the wall. Physically, the momentum thickness is the width of flow at u_0 that would be needed to replace the momentum lost due to the boundary layer. In this work, the momentum thickness is calculated at the free surface in the spanwise direction, mainly to be as away from the influence of the boundary layer that forms near the stream bed. Depth-averaging of the parameter is possible, however, since primary interest is in the momentum thickness in the lateral direction, that the stream bottom may bias the distribution considering that the streams are shallow. The rotation time, T_{rot}, scaled by the ratio of the dead zone width, W, and the boundary layer momentum thickness, θ, is approximately linearly correlated with the Langmuir time scale as shown in figure 6(b) and below,

$$\theta = \int_0^\infty \frac{u}{u_0}\left(1 - \frac{u}{u_0}\right) dy \tag{15}$$

$$\frac{W}{k_e U} = \tau_L \sim 0.5 \frac{W}{\theta}\frac{1}{\overline{\omega}_v} \sim 0.5 \frac{W}{\theta}\frac{2W}{U} \implies k_e \sim \frac{\theta}{W} \tag{16}$$

While the the trend of figure 6(b) is clearly linear for the W cases, the other data points have a significant standard deviation from the linear fit. The important output of this figure is that the slope is approximately 0.5. Using equation 16, this slope implies that the entrainment coefficient, k_e, is related to the ratio of the momentum thickness (θ) to the dead zone width (W). This provides a scaling argument for why experiments (Valentine and Wood 1979; Uijttewaal et al. 2001; Weitbrecht et al. 2008) have consistently found k_e to be in the range $0.01 - 0.03$. Obtaining an approximate Langmuir time scale using equation 16 is straightforward without requiring tracer tests. Only measurements of the upstream momentum thickness (θ) and the average rotation rate (or average vorticity, $\overline{\omega}_v$) are required. The momentum thickness of the upstream boundary layer can be obtained by measuring the mean velocity profile normal to the stream or can be estimated using correlations for boundary layer development based on the flow Reynolds numbers. The rotation time scale can also be obtained by measuring the velocity profile along the center of the mixing layer (U_m) and using equation 13 to obtain the mean circulation and average vorticity within the dead zone. Alternatively, an estimate for average vorticity within the dead zone can be obtained by using equation 14.

TWO REGION MODEL RESULTS

When using the first order model, the Langmuir time scale fully defines the normalized concentration plot and thus could be used to predict the response of a dead zone to changes in the main channel concentration. Figure 7 shows the mean streamlines within the dead zone and an instantaneous passive scalar contour plot at a simulation time of 5000s. It is observed that a single recirculation is present within the dead zone, which has been observed for majority of the test cases studied here. The scalar contour plot, figure 7(b), also shows non-uniformity within the dead zone. The main recirculation eddy separates the dead zone into two regions, the core region of the main eddy where the average velocity is small and the perimeter region where the velocity and mixing are larger. Figure 8 shows the time history of the average scalar concentration for the base case. The temporal evolution of scalar concentration in a perfectly mixed dead zone is exponential as shown in equation 4. On a semi-log plot, an exponential would make a linear trend. Figure 8 shows the temporal evolution of the scalar concentration normalized by the initial concentration within the dead zone. The time is also normalized by the primary zone time scale as shown for three different cases $W/L = 0.345, 0.4, 1.11$. In addition, for the baseline case of $W/L = 0.4$, a linear curve corresponding to the primary zone (which is also close to the Langmuir) time scale is plotted. It is clear from this figure that up to one non-dimensional time unit, the concentration evolution nearly follows the linear evolution, which suggests that the initial scalar evolution is mainly governed by direct exchange between the primary zone and the main stream through the mixing layer. A similar plot was also produced by Weitbrecht et al. (2008) from their experiments. However, figure 8 does show some positive curvature confirming that more than one time scale exists and that the dead zone is not perfectly mixed. It is also important to note that nearly 75-80% of the scalar mass has escaped within the first non-dimensional time unit, similar to the observations by Weitbrecht et al. (2008). The remaining tracer mass exits slowly and involves time scale of a secondary zone thus indicating the need for at least a two-zone model. The predicted results are consistent with recent field measurements conducted by Jackson et al. (2012).

Without a well-mixed dead zone, the first order model is not accurate to completely describe the long-time evolution of the tracer field. As an extension of the first order model and following the method used by Kozerski et al. (2006), the dead zone can be divided into two perfectly mixed CSTRs, one in the perimeter of the main eddy (primary region) and one in the core of the main recirculation (secondary region), see figure 7(b). The primary region, with volume V_p and concentration C_p, exchanges scalar with the main channel based on the exchange volume flow rate, Q_{pm}. In this region, the flow velocity and turbulent diffusivity are large which facilitate rapid mixing. The secondary region, with volume V_s and concentration C_s, exchanges scalar with just the primary region based on the exchange volume flow rate, Q_{ps}. This model does not specify the exact shape of the secondary region, only the volume and the exchange volume flow rates. Using the conservation of mass for a passive scalar, two coupled differential equations (17 and 18), can be derived to model the two regions.

$$\frac{dC_p}{dt} = -\frac{Q_{pm}}{V_p} C_p - \frac{Q_{ps}}{V_p} \left(C_p - C_s\right) \tag{17}$$

$$\frac{dC_s}{dt} = -\frac{Q_{ps}}{V_s} \left(C_s - C_p\right) \tag{18}$$

The governing equations can be solved analytically to obtain,

$$\begin{bmatrix} C_s \\ C_p \end{bmatrix} = k_s \begin{bmatrix} 1 \\ 1 - \frac{\tau_{sp}}{\tau_s} \end{bmatrix} e^{-\frac{t}{\tau_s}} + k_p \begin{bmatrix} 1 \\ 1 - \frac{\tau_{sp}}{\tau_p} \end{bmatrix} e^{-\frac{t}{\tau_p}}, \tag{19}$$

where τ_s and τ_p are the negative reciprocals of the eigenvalues of the system, the vectors on the right hand side are the eigenvectors, and $k_s = \frac{\frac{1}{\tau_p}}{\frac{1}{\tau_p} - \frac{1}{\tau_s}}$, $k_p = \frac{\frac{1}{\tau_s}}{\frac{1}{\tau_s} - \frac{1}{\tau_p}}$ are constants determined by the initial conditions of 1 for both regions. The time scales for scalar exchange between different regions are given as $\tau_{sp} = \frac{V_s}{Q_{ps}}$, $\tau_{pm} = \frac{V_p}{Q_{pm}}$, and $\tau_{ps} = \frac{V_p}{Q_{ps}}$. Then, the time scales for the primary (τ_p) and secondary regions (τ_s) are given by,

$$\tau_p, \, \tau_s = 2 \left[\frac{Q_{pm}}{V_p} + \frac{Q_{ps}}{V_p} + \frac{Q_{ps}}{V_s} \pm \sqrt{\left(\frac{Q_{pm}}{V_p} + \frac{Q_{ps}}{V_p} + \frac{Q_{ps}}{V_s} \right)^2 - \frac{4 Q_{pm} Q_{ps}}{V_p V_s}} \right]^{-1} \tag{20}$$

The mean dead zone concentration is volume weighted summation of the mean concentrations in the primary and secondary regions, $C_{DZ} = \frac{C_s V_s + C_p V_p}{V_p + V_s} = \frac{C_s \tau_{sp} + C_p \tau_{ps}}{\tau_{sp} + \tau_{ps}}$. The mean dead zone concentration can be expressed as,

$$C_{DZ} = \left(1 - k_W\right) e^{-\frac{t}{\tau_s}} + k_W e^{-\frac{t}{\tau_p}}, \quad k_W = \frac{\tau_{sp} \frac{\frac{1}{\tau_s}}{\frac{1}{\tau_s} - \frac{1}{\tau_p}} + \tau_{ps} \frac{\frac{1}{\tau_s}}{\frac{1}{\tau_s} - \frac{1}{\tau_p}} \left(1 - \frac{\tau_{sp}}{\tau_p}\right)}{\tau_{sp} + \tau_{ps}}, \tag{21}$$

where k_W represents a single weighting factor. If it is assumed that $\tau_p << \tau_s$ and $\tau_{sp} \sim \tau_s$, then weighting factor simplifies to,

$$k_W \sim \frac{\tau_{ps}}{\tau_{sp} + \tau_{ps}} = \frac{V_p}{V_p + V_s}, \tag{22}$$

and can be thought of as the ratio of the primary region volume to the entire dead zone volume.

Two Region Model Fitting

Given the three model parameters, τ_p, τ_s, and k_W, the average concentration is known at all times using equation 21. Without a method for determining the model parameters, this model is only a mathmatical exercise. Tuning the model is accomplished by fitting the model to the concentration results from the parametric RANS studies using an optimization procedure. The difference between concentration plots from the model and a RANS simulation is minimized. A MATLAB-based optimization code, SNOPT (Gill et al. 1994), does the minimization using a robust implementation of a sequential quadratic programming algorithm for nonlinear problems.

Using SNOPT (Gill et al. 1994), τ_p, τ_s, and k_W are varied to minimize the square of the difference between the temporal evolution of mean concentration curves in the dead zone obtained from the RANS simulation and the two region model. The weighting factor is constrained to be between 0.25 and 0.75 to ensure that both optimized time scales have a significant influence on the concentration plot. A maximum error of 2.05% was obtained between the mean dead zone concentration from the model and the RANS study (see Drost (2012) for details on the optimization procedure). These results show that this model can accurately fit the RANS results a posteriori.

The average k_W value was found to be 0.55 with a standard deviation of 0.17, indicating that the dead zone volume is almost equally split between the primary and secondary regions. The primary time scale, τ_p, obtained from the two-region model was compared with the Langmuir time scale as shown in figure 9(a). It is observed that τ_L and τ_p are roughly on the same order and show direct linear correlation between them. The primary region time scale compared with the rotational time- scale in the dead zone, T_{rot}, also shows a linear fit (figure 9(b)) indicating that as the rate of rotation within the dead zone is increased, the primary region residence time decreases. This suggests that the primary region time scale, τ_p, provides a good estimate of the Langmuir time scale. Both time scales are correlated to rotation of the dead zone. This matches the reasoning for creating the two region model, that primary region seemed to contain the majority of the recirculating fluid.

The secondary region time scale, τ_s, was found to be generally two to four times larger than the primary region time scale for all cases verifying the presence of at least two distinct time scales within the dead zone. The larger time scale, τ_s governs the asymptotic behavior of the concentration plot in time. The separation of time scales causes τ_p dominating the exchange with the main stream at early times when the dead zone is approximately perfectly mixed. At late times, τ_s limits the exchange rate. This is similar to the multiple time scales observed by Uijttewaal et al. (2001).

The two region model has been shown to be able to fit RANS results with small error. However, to make the model predictive, the model parameters need to be estimated based on dead zone geometry and flow conditions. Accordingly, the primary and secondary region time scales can be related to the geometric paramters, L, W, D, and free-stream average velocity, U, by forming non-dimensional groups and assuming a power law relationship. The convective time scale T_{conv} is used for non-dimensionalization as it is the smallest possible time scale in the system.

$$\frac{\tau_p(\text{or } \tau_s)}{T_{conv}} = a\left(\frac{W}{L}\right)^b \left(\frac{W}{D}\right)^c \left(\frac{WU}{\nu}\right)^d \tag{23}$$

The specific non-dimensionalization groups are not unique, but any other combination will lead to equivalent results. Using four independent simulations and this power law, four equations define the constants a, b, c, and d. Averaging the results from all the independent groups of four from the 17 simulations, gives the relationships,

$$\frac{\tau_p}{T_{conv}} \sim 15 \left(\frac{W^3 D}{L^3}\frac{U}{\nu}\right)^{\frac{1}{4}} = 15 \left(\frac{W}{L}\right)^{3/4} \left(\frac{UD}{\nu}\right)^{\frac{1}{4}} \tag{24}$$

$$\frac{\tau_s}{T_{conv}} \sim 170 \left(\frac{W^4}{L^3 D}\right)^{\frac{1}{2}} = 170 \left(\frac{W}{L}\right)^{\frac{3}{2}} \left(\frac{W}{D}\right)^{\frac{1}{2}} \tag{25}$$

Using the approximate nondimensional relationships, the model parameters are plotted in figures 10(a) and 10(b). Each plot has symbols for cases that vary L, W, D, and U compared to the base case. Cases 6 and 7 (as shown in table 1) were considered outliers. For these cases L is varied such that the aspect ratio $W/L \sim 1$. Above an aspect ratio of one, the overall flow structure has been shown to change to a multiple eddy configuration. This transition to another type of flow field may not follow the same trends as lower aspect ratio dead zones. These cases were not used when determining the exponents.

The non-dimensional primary region time scale is cast as an effective Reynolds number $(\frac{W^3 D}{L^3}\frac{U}{\nu})$, with the length scale given as W^3D/L^3. This relation can also be thought of as a combinations of dependence on the geometry, W/L, and flow, Re_D, conditions. As seen from figure 10(a), the non-dimensional primary region time scale increases with increase in the aspect ratio and the Reynolds number based on the depth. It should be noted that this time scale is normalized by the normalized by the flow time scale L/U. The primary zone time scale decreases with increasing velocity, however, the ratio of time scales increases with increasing Re_D. This result is also consistent with the predictive relationship developed by Jackson et al. (2013) using laboratory-scale experiments on isolated dead-zones in idealized semi-circular configurations. While this trend in the prsent work is empircally derived, its form can be attributed to physical phenomenon. It is understandable that the aspect ratio has a large influence as experiments have shown that it largely determines the shape and quantity of eddies in the dead zone. The time scale ratio weakly depends on D. This result is consistent with Constantinescu et al. (2009) and Hinterberger et al. (2007) who showed this shallow flow to have weak dependence on the depth. Uijttewaal et al. (2001) and Weitbrecht et al. (2008) also showed exchange velocities to be roughly proportional to

U. Equation 24 implies that the exchange velocity depends on $U^{0.8}$.

When analyzing the secondary region time scale, the Reynolds number had a very small exponent meaning that the quantity does not significantly depend on U and only geometric ratios were considered. The secondary time scale ratio, as shown in equation 25, scales with geometry only. A lack of dependence on U may be attributed to the small average velocities within the secondary region and small turbulent diffusion across the region that determines the time scale. Similar to τ_p, the secondary time scale is heavily dependent on the aspect ratio and slightly dependent on the depth.

SUMMARY AND CONCLUSIONS

Parametric studies varying the length, depth, width, and the averaged free-stream velocity were performed on idealized dead zones with rectangular cavity using three dimensional Reynolds averaged Navier Stokes simulations based on the experimentally validated k-ω model. The main purpose of this fundamental numerical study was to identify scales that are important to characterize the residence times in lateral storage zones occurring in small streams. In this study, seventeen cases were investigated wherein the aspect ratio, $0.4 \leq W/L \leq 1.1$, and Reynolds number based on the width, $5000 \leq Re_D \leq 20300$, were varied over a range typically observed in small streams. For this range, the main flowfield is characterized by an open cavity flow consisting of a mixing layer that spans the entire length of the dead zone and a large main recirculation region within the dead zone.

In addition to showing good validation with available experimental data, our main contributions of the present work are:

1. correlating the hydraulic residence time (the Langmuir time scale) to the rotation time scale within the dead zone, a quantity that can be easily measured in the field,

2. developing a new scaling based on the momentum thickness of the upstream boundary layer that makes the entrainment coefficient on the order of 1, instead of traditional values of 0.01 with large variability,

3. indicating an existence of two time scales within the dead zone for the conditions considered (subcritical isolated dead zone for $0.4 \leq W/L \leq 1$),

4. developing a two-zone model with parameters calibrated to predict residence time scales through power law correlations involving the dead zone geometric quantities and flow Reynolds number.

Based on the flow features observed, it was hypothesized that the hydraulic residence time (or the Langmuir time scale) may depend on the average rotation rate within the dead zone, the geometric scales, and the characteristics of the upstream boundary layer that drives the flow and mixing layer over the dead zone. It was shown that the Langmuir time scale is inversely proportional to the average rotation rate (or average vorticity) within the dead zone. The entrainment coefficient (k_e), used to relate the exchange velocity to the average free-stream velocity was shown to be on the order of θ/W, the ratio of the upstream boundary layer momentum thickeness (θ) to the width (W) of the dead zone.

For a perfectly mixed dead zone, the Langmuir time scale completely describes the residence time of the dead zone. However, the numerical simulations show that the dead zone is not perfectly mixed. The core region of the main recirculation region retains scalar longer than the perimeter region. This nonuniformity indicates the presence of multiple time scales within the dead zone that can be approximated by a two region model, a primary perimeter region that interacts with the mixing layer and exchanges scalar with the free-stream directly and a secondary core region that interacts with the primary region. The regions were approximated as continuously stirred tank reactors with mass transport between them. The resultant two-region model involved three parameters, the primary region time scale, the secondary region time scale, and a scaling factor approximately proportional to the ratio of the primary region volume to the dead zone volume. These parameters were obtained from the RANS data and using SNOPT optimization procedure that fits the model to the RANS concentration curves. The fitting error was less than 2%.

Fitting the two region model to the RANS results showed that the primary region time scale is directly proportional to the Langmuir time scale, indicating that the primary region is well mixed and also dominated by mixing due to rapid rotation as well as turbulent diffusion. The secondary region time scale was generally two to four times larger than the Langmuir time scale and determines the late time behavior of the dead zone. The larger secondary region time scale is characteristic of the lower turbulent diffusivity within the core region. This comparison also suggests that time scale determined using field tracer tests with concentration measurements taken uniformly over the dead zone can result in an apparently larger Langmuir time scale owing to the slower mixing processes within the secondary region. This observation was consistent with the field measurements on natural dead zones as noted by Jackson et al. (2012).

Additional power law relationships were formed to correlate the three model parameters to the basic geometric and flow parameters. The trends for the primary and secondary time scales collapsed and would therefore allow the time scales to be predicted from basic geometric and flow measurements of a dead zone. The primary time scale was found to be well correlated with the aspect ratio, $(W/L)^{3/4}$, and Reynolds number based on the depth, $(UD/\nu)^{1/4}$. An effective length scale, W^3D/L^3, was defined to describe the primary region time scale suggesting dependence on the aspect ratio as well as the depth of the dead zone. The secondary region time scale was found to be dependent on only geometric parameters. A lack of dependence on U may be attributed to the small average velocities within the secondary region and small turbulent diffusion. The average value for the weighting factor was found to be 0.55 with a standard deviation of 0.17, indicating that the dead zone volume is almost equally split between the primary and secondary regions.

The predictive capability of these results is limited to the range of parameters studied wherein the main flowfield is characterized by an open cavity flow consisting of a mixing layer that spans the entire length of the dead zone and a large main recirculation region within the dead zone. Such conditions were obtained for shallow sub-critical dead zones ($0.16 < \mathrm{Fr} < 0.32$) with aspect ratios $0.3 \leq W/L \leq 1$ over relatively low Reynolds numbers ($5000 \leq$

$Re_D \leq 20300$) based on the stream depth. For these conditions, additional fundamental work involving flume studies as well as high-fidelity large-eddy simulation on idealized, isolated dead zones are needed to corroborate the present findings.

ACKNOWLEDGEMENTS

This work was supported by the National Science Foundation, EAR 0943570.

APPENDIX I. NOTATION

The following symbols are used in this paper:

$A =$ Planform dead zone area
$C =$ Scalar concentration where $_0$=initial, $_{DZ}$=dead zone, $_{mc}$=main channel, $_p$=primary region, and $_s$=secondary region
$\Delta C =$ Concentration difference between the dead zone and the main channel
$\Gamma =$ Circulation calculated around a closed loop
$D =$ Dead zone depth
$D_T =$ Turbulent scalar diffusivity
$E =$ Entrainment velocity
$\theta =$ Momentum thickness
$Fr =$ Froude number
$k_e =$ Entrainment coefficient
$k_p =$ Eigenvector for the primary region term
$k_s =$ Eigenvector for the secondary region term
$k_W =$ Two region model weighting factor
$k =$ Turbulent kinetic energy
$l =$ Closed path length variable for the calculation of circulation
$L =$ Dead zone length in the streamwise direction
$M =$ Mass of scalar in the dead zone
$\nu =$ Kinematic viscosity
$\nu_T =$ Turbulent diffusivity of the fluid
$\omega =$ Turbulent dissipation rate
$\omega_v =$ Vorticity
$\Omega =$ Average rotatoin rate in the dead zone
$P =$ Fluid pressure
$Q =$ Volumetric flow rate where $_{pm}$=flow between the primary region and main channel and $_{ps}$=flow between the primary and secondary regions
$Re_D =$ Reynolds number based on the dead zone depth
$\rho =$ Fluid density
$Sc =$ Scalar Schmidt number
$Sc_T =$ Turbulent scalar Schmidt number
$t =$ Time
$T =$ Dead zone time scale where $_0$=asymptotic time scale, $_{avg}$=average time scale, $_{conv}$=convective time scale, and $_{rot}$=rotation time scale
$\tau_{ij} =$ Reynolds stress tensor
τ Dead zone time scale where $_L$=Langmuir time scale, $_p$=primary region time scale, $_s$=secondary region time scale, $_{pm}$=primary region to main channel time scale, $_{ps}$=primary region to secondary region time scale, and $_{sp}$=secondary region to primary region time scale
$u_i =$ Fluid velocity vector
u_0 Velocity outside the boundary layer
$U =$ Average main channel velocity
$U_m =$ Mixing layer characteristic velocity

$V =$ Dead zone volume where $_p$=primary region volume and $_s$=secondary region volume
$W =$ Dead zone width
$x_i =$ Position vector
$\Delta X^+ =$ Streamwise position in wall units
$\Delta Y^+ =$ Depth position in wall units
$\Delta Z^+ =$ Spanwise position in wall units

APPENDIX II. REFERENCES

Baik, J., Kim, J., and Fernando, H. (2003). “A cfd model for simulating urban flow and dispersion.” *Journal of Applied Meteorology*, 42(11), 1636–1648.

Bellucci, A., Buffoni, G., Griffa, A., and Zambianchi, E. (2001). “Estimation of residence times in semi-enclosed basins with steady flows.” *Dynamics of atmospheres and oceans*, 33(3), 201–218.

Briggs, M., Gooseff, M., Arp, C., and Baker, M. (2009). “A method for estimating surface transient storage parameters for streams with concurrent hyporheic storage.” *Water Resources Research*, 45(null), W00D27.

Chang, K., Constantinescu, G., and Park, S. (2006). “Analysis of the flow and mass transfer processes for the incompressible flow past an open cavity with a laminar and a fully turbulent incoming boundary layer.” *Journal of Fluid Mechanics*, 561(4), 113–145.

Constantinescu, G., Sukhodolov, A., and McCoy, A. (2009). “Mass exchange in a shallow channel flow with a series of groynes: Les study and comparison with laboratory and field experiments.” *Environmental fluid mechanics*, 9(6), 587–615.

Drost, K. (2012). “Rans and les predictions of turbulent scalar transport in dead zones of natural streams.” *M.S. Thesis, Oregon State University, Corvallis, OR.*

Engelhardt, C., Krüger, A., Sukhodolov, A., and Nicklisch, A. (2004). “A study of phytoplankton spatial distributions, flow structure and characteristics of mixing in a river reach with groynes.” *Journal of plankton research*, 26(11), 1351–1366.

Gill, P., Murray, W., and Saunders, A. (1994). “Snopt 5.3 user manual.” *Department of Mathematics, University of California, San Diego.*

Gooseff, M., LaNier, J., Haggerty, R., and Kokkeler, K. (2005). “Determining in-channel (dead zone) transient storage by comparing solute transport in a bedrock channel–alluvial channel sequence, oregon.” *Water Resources Research*, 41, W06014.

Gualtieri, C., Jiménez, P., and Rodríguez, J. (2010). “Modelling turbulence and solute transport in a square dead zone.” *IAHR 2010 European Congress.*

Hinterberger, C., Fröhlich, J., and Rodi, W. (2007). "Three-dimensional and depth-averaged large-eddy simulations of some shallow water flows." *Journal of Hydraulic Engineering*, 133, 857.

Jackson, T. R., Haggerty, R., Apte, S. V., Coleman, A., and Drost, K. J. (2012). "Defining and measuring the mean residence time of lateral surface transient storage zones in small streams." *Water Resources Research*, 48(10), W10501.

Jackson, T. R., Haggerty, R., Apte, S. V., and O'Connor, B. L. (2013). "A mean residence time relationship for lateral cavities in gravel-bed rivers and streams: Incorporating streambed roughness and cavity shape." *Water Resources Research*, 49(6), 3642–3650.

Kimura, I. and Hosoda, T. (1997a). "Fundamental properties of flows in open channels with dead zone." *Journal of Hydraulic Engineering*, 123, 98.

Kimura, I. and Hosoda, T. (1997b). "Fundamental properties of flows in open channels with dead zone." *Journal of Hydraulic Engineering*, 123(2), 98–107.

Koseff, J. and Street, R. (1984). "The lid-driven cavity flow: a synthesis of qualitative and quantitative observations." *Journal of fluids engineering*, 106, 390.

Kozerski, H., Schwartz, R., and Hintze, T. (2006). "Tracer measurements in groyne fields for the quantification of mean hydraulic residence times and of the exchange with the stream." *Acta hydrochimica et hydrobiologica*, 34(3), 188–200.

Kurzke, M., Weitbrecht, V., and Jirka, G. (2002). "Laboratory concentration measurements for determination of mass exchange between groin fields and main stream." *River Flow*, Vol. 1. 369–376.

Langmuir, I. (1908). "The velocity of reactions in gases moving through heated vessels and the effect of convection and diffusion.." *Journal of the American Chemical Society*, 30(11), 1742–1754.

Lawson, S. and Barakos, G. (2011). "Review of numerical simulations for high-speed, turbulent cavity flows." *Progress in Aerospace Sciences*.

Levenspiel, O. (1967). *Chemical Reaction Engineering: An Introduction to the Design of*

Chemical Reactors. John Wiley & Sons.

Lien, K., Monty, J., Chong, M., and Ooi, A. (2004). "The entrance length for fully developed turbulent channel flow." *15th Australasian Fluid Mechanics Conference, The University of Sydney, Ausralia*.

Lin, J. and Rockwell, D. (2001). "Organized oscillations of initially turbulent flow past a cavity." *AIAA Journal*, 39(6), 1139–1151.

Liu, X. and Katz, J. (2008). "Cavitation phenomena occurring due to interaction of shear layer vortices with the trailing corner of a two-dimensional open cavity." *Physics of fluids*, 20(4), 41702–41702.

McCoy, A., Constantinescu, G., Weber, L., et al. (2008). "Numerical investigation of flow hydrodynamics in a channel with a series of groynes." *Journal of Hydraulic Engineering*, 134, 157–172.

Nakayama, A. and Yokojima, S. (2003). "Modeling free-surface fluctuation effects for calculation of turbulent open-channel flows." *Environmental Fluid Mechanics*, 3(1), 1–21.

Nauman, E. (2008). "Residence time theory." *Industrial & Engineering Chemistry Research*, 47(10), 3752–3766.

Santiago, J., Martilli, A., and Martín, F. (2007). "Cfd simulation of airflow over a regular array of cubes. part i: Three-dimensional simulation of the flow and validation with wind-tunnel measurements." *Boundary-layer meteorology*, 122(3), 609–634.

Shankar, P. and Deshpande, M. (2000). "Fluid mechanics in the driven cavity." *Annual Review of Fluid Mechanics*, 32(1), 93–136.

Thackston, E. and Schnelle, K. (1970). "Predicting effects of dead zones on stream mixing." *Journal of the Sanitary Engineering Division*, 96(SA2), 319–331.

Uijttewaal, W., Lehmann, D., and Van Mazijk, A. (2001). "Exchange processes between a river and its groyne fields: Model experiments." *Journal of Hydraulic Engineering*, 127, 928.

User Guide (2009). "Star-ccm+ version 4.04. 011. CD-ADAPCO.

Valentine, E. and Wood, I. (1977). “Longitudinal dispersion with dead zones.” *Journal of the Hydraulics Division*, 103(9), 975–990.

Valentine, E. and Wood, I. (1979). “Dispersion in rough rectangular channels.” *Journal of the Hydraulics Division*, 105(12), 1537–1553.

Weitbrecht, V. and Jirka, G. (2001). “Flow patterns and exchange processes in dead zones of rivers.” *Proceedings of the Congress-International Association for Hydraulic Research.* 439–445.

Weitbrecht, V., Socolofsky, S., Jirka, G., et al. (2008). “Experiments on mass exchange between groin fields and main stream in rivers.” *Journal of Hydraulic Engineering*, 134, 173–183.

List of Tables

TABLE 1. List of parametric study cases and time scale results.

Case	W [m]	L [m]	D [m]	U [$\frac{m}{s}$]	τ_L	τ_p	τ_s	k_W	Fr
Base	0.5	1.25	0.046	0.221	397.2	457.4	1086.3	0.669	0.32
2	0.5	1.45	0.046	0.221	350.1	372.7	808.5	0.350	0.32
3	0.5	1.05	0.046	0.221	426.6	408.0	1148.0	0.637	0.32
4	0.5	0.85	0.046	0.221	454.4	410.6	1275.1	0.691	0.32
5	0.5	0.65	0.046	0.221	438.1	414.5	1331.9	0.747	0.32
6	0.5	0.55	0.046	0.221	447.1	403.3	1115.3	0.745	0.32
7	0.5	0.45	0.046	0.221	498.4	347.7	711.4	0.520	0.32
8	0.5	1.25	0.046	0.248	349.3	402.1	909.1	0.664	0.32
9	0.5	1.25	0.046	0.193	429.4	502.8	1262.1	0.686	0.287
10	0.5	1.25	0.046	0.165	484.8	584.4	1449.0	0.645	0.245
11	0.5	1.25	0.046	0.110	671.3	593.6	1643.6	0.291	0.163
12	1.25	1.25	0.046	0.221	819.3	838.2	4767.9	0.549	0.32
13	1	1.25	0.046	0.221	667.6	724.3	4123.8	0.594	0.32
14	0.75	1.25	0.046	0.221	516.6	608.0	3284.0	0.674	0.32
15	0.5	1.25	0.092	0.221	494.1	470.7	584.5	0.250	0.23
16	0.5	1.25	0.063	0.221	478.0	453.2	612.8	0.250	0.28
17	0.5	1.25	0.023	0.221	149.7	372.1	1243.4	0.428	0.46

List of Figures

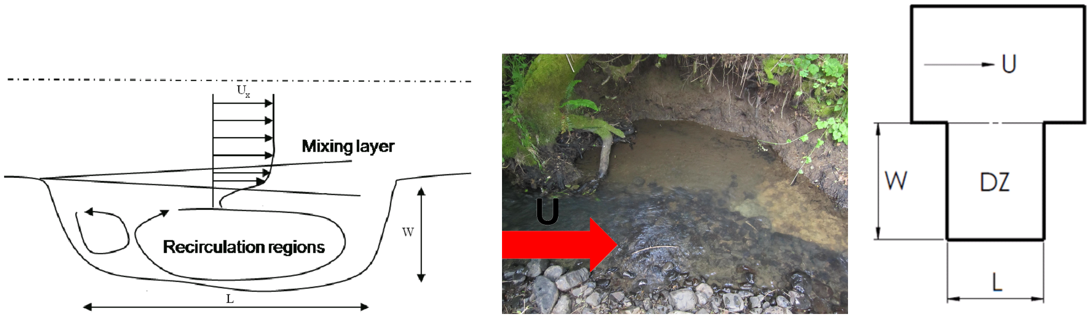

(a) (b) (c)

FIG. 1. Dead zones types, flow features and geometric parameters: (a) planview schematic of a typical dead zone showing the mixing layer and recirculation regions, (b) a photograph of natural dead zone (courtesy T. R. Jackson, unpublished.), (c) planview showing the definitions of ideal dead zone parameters.

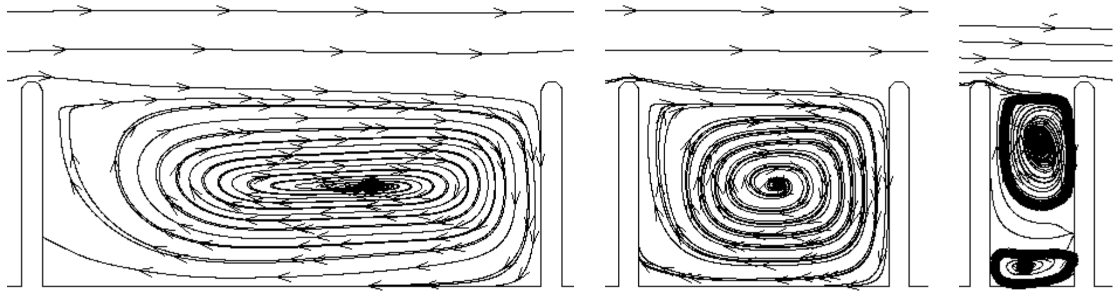

(a) W/L=0.4 (b) W/L=0.77 (c) W/L=2

FIG. 2. Streamlines at the free surface in a dead zone after the shear layer is fully developed for different W/L corresponding to the experiments by Weitbrecht *et al.* (2008).

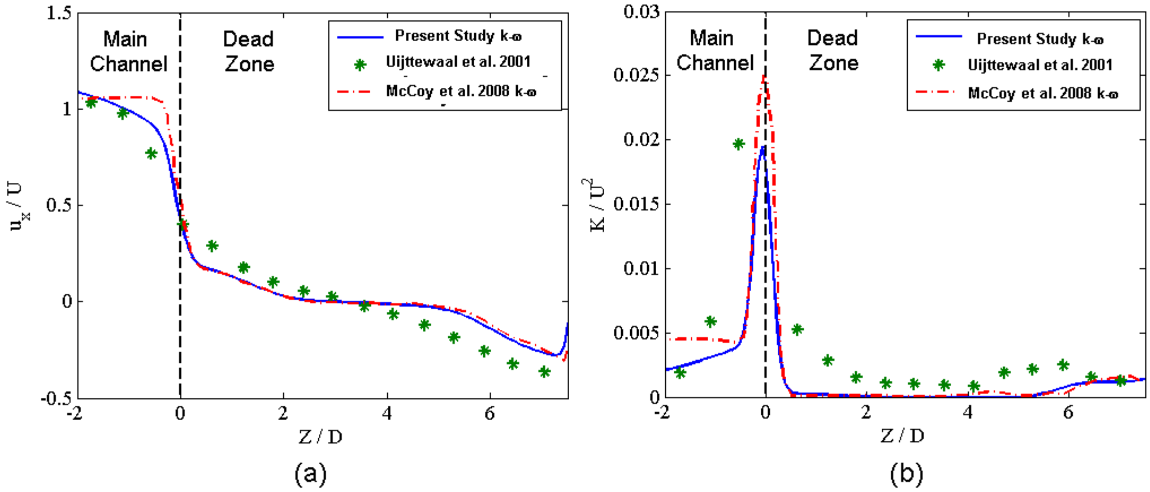

FIG. 3. Spanwise profiles: (a) Streamwise velocity profile corresponding to the $x = 24$, (b) turbulent kinetic energy corresponding to the $x = 25$.

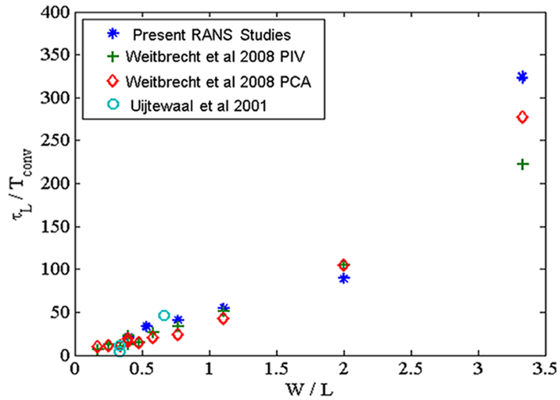

FIG. 4. Comparison of predicted Langmuir time scale with experimental results from Uijttewaal *et al.* **(2001) and Weitbrecht** *et al.* **(2008) for series of dead zones with different aspect ratios.**

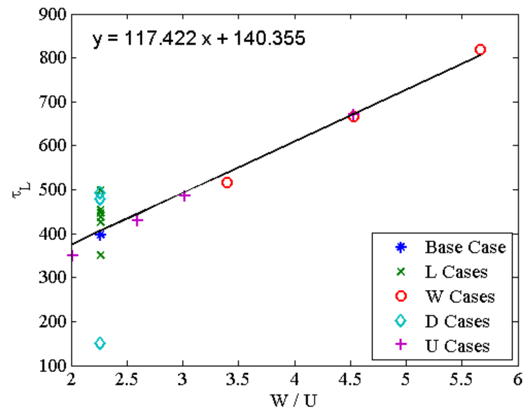

FIG. 5. The Langmuir time scale, τ_L versus W/U for all cases. Inverse slope is equal to the entrainment coefficeint ($1/k_e$), R^2 for the fit is 0.72.

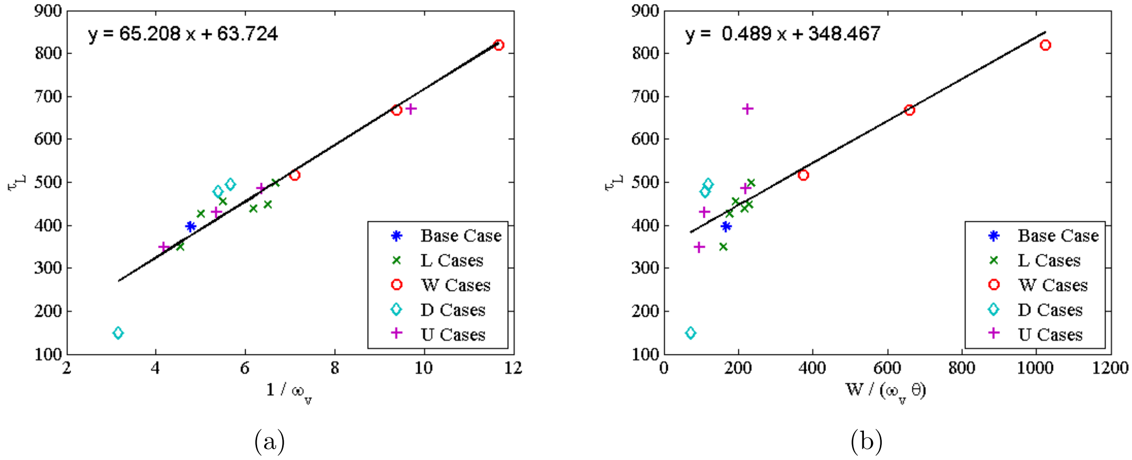

FIG. 6. The Langmuir time scale versus the rotation time scale for all cases: (a) τ_L versus $1/\overline{\omega}_v$ (R^2 for fit is 0.92), (b) τ_L versus $W/\theta\overline{\omega}_v$ (R^2 for fit is 0.74).

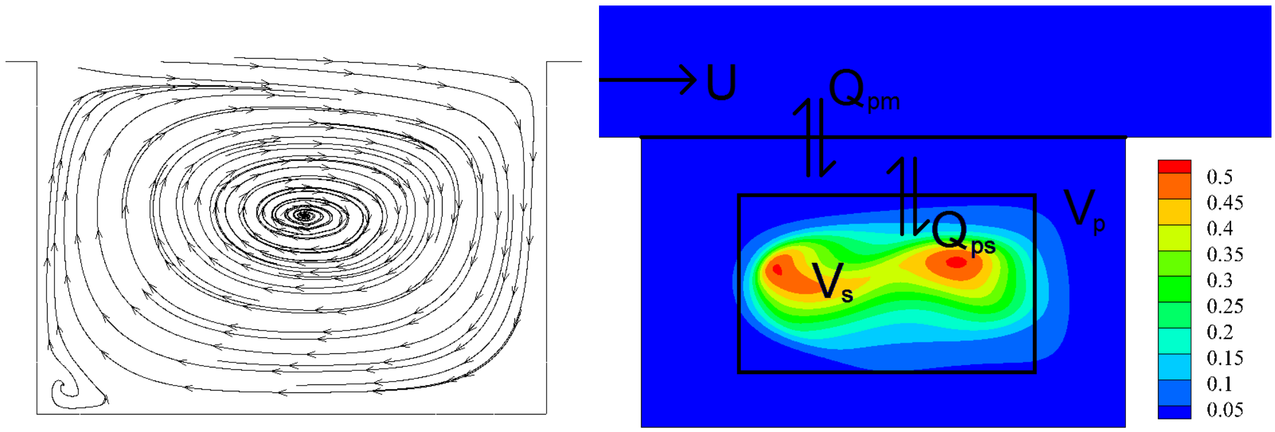

(a) (b)

FIG. 7. Flowfield and passive scalar in case # 14 $W/L = 0.6$: (a) streamlines, (b) passive scalar plot at late times showing non-uniform mixing within the dead zone. Schematic of two-region model is also shown.

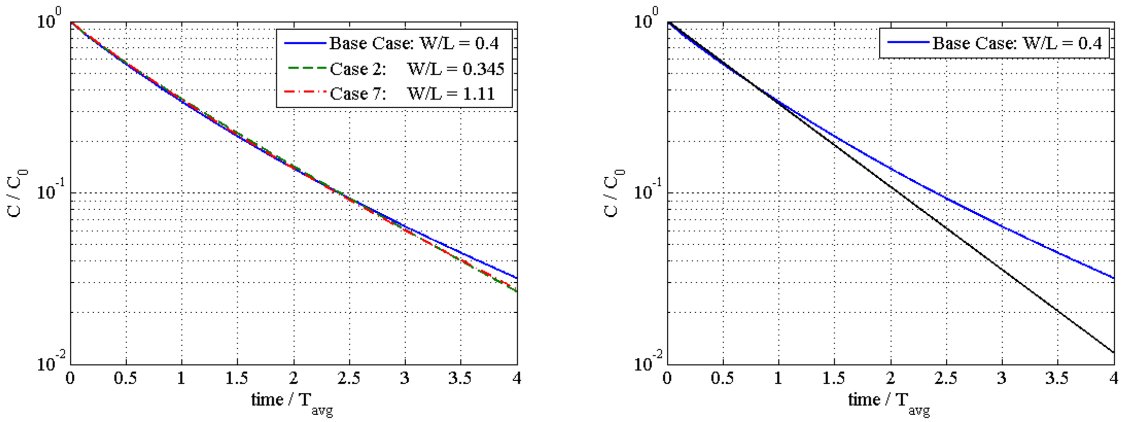

(a) (b)

FIG. 8. Temporal evolution of the passive scalar concentration for different W/L on a semi-log axis. Time is normalized by the primary zone time scale: (a) different cases, (b) linear fit for the baseline case.

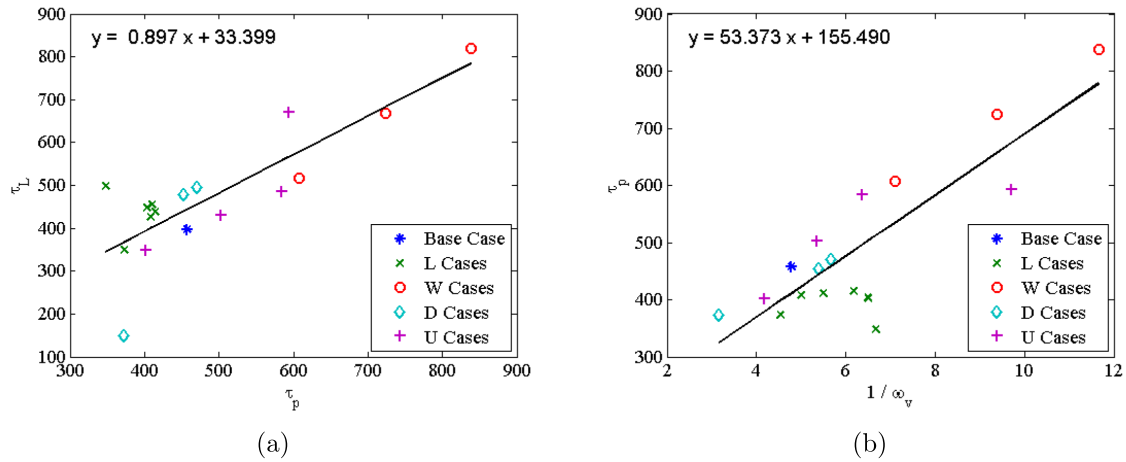

FIG. 9. Comparison of the Langmuir time scale, τ_L, the primary region time scale, τ_p, and the rotational time scale, $T_{rot} = 2/\overline{\omega}_v$: (a) τ_L versus τ_p (R^2 for fit is 0.68), (b) τ_p versus $1/\overline{\omega}_v(= T_{rot}/2)$ (R^2 for fit is 0.73).

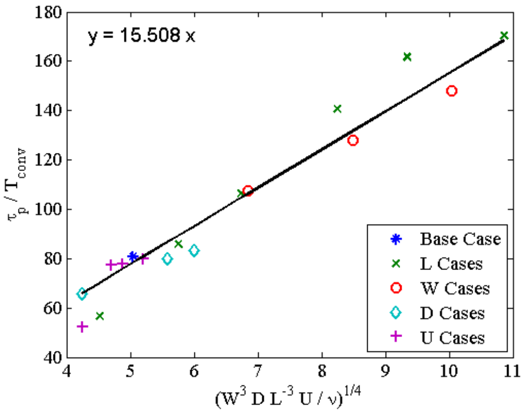

(a)

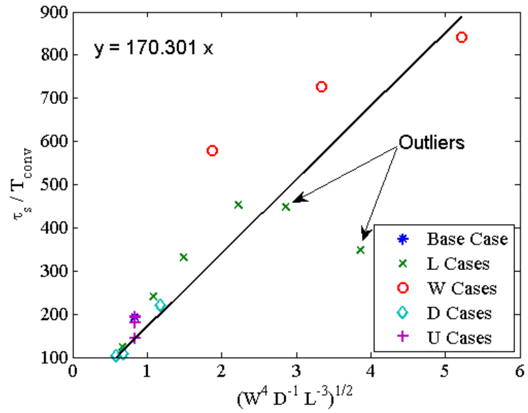

(b)

FIG. 10. Power law relation for non-dimensionalized primary and secondary time scales with the geometric parameters and Reynolds number. (a) τ_p/T_{conv} (R^2 for fit is 0.95), (b) τ_s/T_{conv} (R^2 for fit is 0.73).